The Journal of Chemical Physics

RESEARCH ARTICLE | JUNE 24 2015

Stability of micro-Cassie states on rough substrates

Zhenjiang Guo; Yawei Liu; Detlef Lohse; Xuehua Zhang; Xianren Zhang

J. Chem. Phys. 142, 244704 (2015)
https://doi.org/10.1063/1.4922905

AIP Publishing

Stability of micro-Cassie states on rough substrates

Zhenjiang Guo,[1] Yawei Liu,[1] Detlef Lohse,[2] Xuehua Zhang,[2,3] and Xianren Zhang[1]
[1]*State Key Laboratory of Organic-Inorganic Composites, Beijing University of Chemical Technology, Beijing 100029, China*
[2]*Physics of Fluids group, Department of Science and Technology, Mesa+ Institute, and J. M. Burgers Centre for Fluid Dynamics, University of Twente, P.O. Box 217, 7500 AE Enschede, The Netherlands*
[3]*School of Civil, Environmental and Chemical Engineering, RMIT University, Melbourne, VIC 3001, Australia*

(Received 3 April 2015; accepted 12 June 2015; published online 24 June 2015)

We numerically study different forms of nanoscale gaseous domains on a model for rough surfaces. Our calculations based on the constrained lattice density functional theory show that the interconnectivity of pores surrounded by neighboring nanoposts, which model the surface roughness, leads to the formation of stable microscopic Cassie states. We investigate the dependence of the stability of the micro-Cassie states on substrate roughness, fluid-solid interaction, and chemical potential and then address the differences between the origin of the micro-Cassie states and that of surface nanobubbles within similar models. Finally, we show that the micro-Cassie states share some features with experimentally observed micropancakes at solid-water interfaces. © *2015 AIP Publishing LLC.* [http://dx.doi.org/10.1063/1.4922905]

I. INTRODUCTION

The existence of surface nanoscale bubbles is considered to be surprising because of their long term stability.[1–3] They live for hours, which could not be explained by classical nucleation theory (CNT).[4–6] Several mechanisms, such as a dynamic equilibrium model,[7–9] a contamination layer model,[10–12] and a high density nanobubble model,[13] were proposed to account for their stability. Meanwhile, it is understood that the interplay between contact line pinning and gas oversaturation of the liquid accounts for the surface nanobubble stability.[14–18]

In fact, surface nanobubbles are not the only gaseous state found on solid-liquid interfaces. In 2006, Zhang *et al.* experimentally found that another form of gaseous state exists, which is a quasi-two-dimensional, pancake-like gas layer at the aqueous interface of highly oriented pyrolytic graphite (HOPG).[19] The flat gas layers are of a thickness of 1-5 nm and a lateral size up to several micrometers.[20] Because of their morphological characteristics the gas layers are often called "micropancakes." Compared to surface nanobubbles, micropancakes show a relatively lower stability towards a decrease of the surface tension or to temperature changes. They have been observed on several crystalline substrates but not on octadecyltrimethylchlorosilane-coated silicon (OTS-SI) and hydrophobilized gold surfaces.[19] In some cases, surface nanobubbles were observed to sit on the top of the micropancakes, forming nanobubble-micropancake composites.[19] Because of their unusual characteristics, which are very different from surface nanobubbles, the mechanism of micropancake stability presumably is different from that of surface nanobubbles.[14–18] Various speculations on the origin of micropancake stability exist,[13,19–31] including making contamination responsible[23] or arguing that micropancakes simply correspond to a high gas density achieved by some sort of condensate.[13,22,24,25] However, no consensus has been reached and none of the assumptions seems to be consistent with all experimental observations, perhaps because there may be different sorts of micropancakes.

On *macroscopic* scale, it is well known that a structured hydrophobic substrate (i.e., a superhydrophobic substrate) in contact with water can stay either in a Cassie state (gaseous pockets are trapped inside the substrate roughness) or in a Wenzel state (water wets the roughness), strongly depending on the surface structures across macroscopic and microscopic scales. In analogy, we expect that a stable form of nanoscale gaseous domains at the solid-liquid interface is also closely related to the features of surface structures even down to very small scales, and the stable form may undergo a transition from one to another state in response to the change of surface features.

In this work, we use the constrained lattice density functional theory (CLDFT)[6,32–40] to investigate possible gaseous states stabilized by different substrate roughness, focusing on their stability. The system is found to be either in a micro-Cassie state or in a micro-Wenzel state, and we will work out the phase space when the gaseous states are in the respective forms.

II. MODEL AND METHODS

In LDFT, the grand potential can be expressed as

$$\Omega = k_B T \sum_i [\rho_i \ln \rho_i + (1-\rho_i)\ln(1-\rho_i)] - \frac{\varepsilon_{ff}}{2}\sum_i \sum_a \rho_i \rho_{i+a} + \sum_i \rho_i(\varphi_i - \mu), \quad (1)$$

where k_B is the Boltzmann constant, T is the absolute temperature, ρ_i is the local density at site i, ε_{ff} and ε_{sf} are the fluid-fluid interaction strength and that for solid-fluid, respectively, and φ_i represents the sum of fluid-solid interaction (ε_{sf}) exerted on site

i. At a constant chemical potential, the density distribution at equilibrium (i.e., at a stable or metastable state) can be obtained by solving $\frac{\partial \Omega}{\partial \rho_i} = 0$.

The constrained LDFT is a new method which introduces a functional χ_i defined as $\chi_i = \begin{cases} 0, & \rho_i < 0.5 \quad i \in vapor \\ 1, & \rho_i > 0.5 \quad i \in liquid \end{cases}$ to distinguish the liquid phase from vapor phase.[14,15,32,35,36,38,41–44] The constraint on the volume of droplets/bubbles reads

$$\Omega' = \kappa \left[N_L^0 - N_L \right] \tag{2}$$

in which κ is the Lagrange multiplier, N_L^0 is the given volume, and $N_L = \sum_i \chi_i$. The constrained grand potential is defined as

$$\begin{aligned} \Omega^C = \Omega + \Omega' = k_B T \sum_i \left[\rho_i \ln \rho_i + (1 - \rho_i) \ln (1 - \rho_i) \right] \\ - \frac{\varepsilon_{ff}}{2} \sum_i \sum_a \rho_i \rho_{i+a} + \sum_i \rho_i (\varphi_i - \mu) \\ + \kappa \left[N_L^0 - \sum_i \chi_i \right]. \end{aligned} \tag{3}$$

Through solving the equations $\frac{\partial \Omega^C}{\partial \rho_i} = 0$ and $\frac{\partial \Omega^C}{\partial \kappa} = 0$, the local density ρ_i is obtained as

$$\rho_i = \frac{1}{1 + \exp\left(\varepsilon_{ff} \sum_a \rho_{i+a} - \varphi_i + \mu + \kappa \frac{\partial \chi_i}{\partial \rho_i} \right)} \quad \forall i. \tag{4}$$

Finally, the local density ρ_i and the Lagrange multiplier κ can be obtained by an iteration algorithm.[36,37,39]

The size of the simulation box that we chose is $70 \times 70 \times 70$ in lattice unit. Periodic boundaries conditions were employed in x- and y-directions, while a mirror boundary condition was used in z-direction. The substrate was at the bottom of the box normal to the z-direction. In our simulations, the substrate was covered with a number of posts, in order to represent a surface with same nanoscale roughness. In order to characterize and quantify the morphology of the substrate, we used the ratio of the area covered by posts to the total area. Unless differently specified, the posts were of size 1×1 and height 5, and ε_{ff} and ε_{sf} were set, respectively, to 1.0 and 0.3, implying that the substrate was hydrophobic. We realize that the aspect ratio height/width of the post is much larger than realistic morphology would be, but the aim of the study is to show possible phenomena rather than aiming at quantitative agreement with experiments.

In our work, we used reduced units. The reduced temperature T^* and the chemical potential μ^* are defined as $T^* = k_B T/\varepsilon_{ff}$ and $\mu^* = \mu/\varepsilon_{ff}$, respectively, in which ε_{ff} is the fluid-fluid interaction strength. The reduced distance is defined as $r^* = r/\sigma$ with σ the lattice spacing. Hereafter, the superscript asterisk was omitted to simplify the description. Except that several simulations were performed at $T = 1.0$ to confirm our main results, for all simulation results presented here the temperature was set to $T = 0.8$.

III. RESULTS AND DISCUSSION

A. Stability mechanism of micro-Cassie states

In our simulations, we first constructed a substrate with a number of randomly placed posts to represent the surface with nanoscale roughness [Fig. 1(b)]. We set the ratio of the area covered by the posts to the total area of the substrate to be 0.06 (see Fig. 1), i.e., 6% of the solid surface was covered by posts. For the simple cubic lattice gas, the chemical potential for vapor-liquid coexistence is at $\mu_C = -3.000$. Hence, in most cases, we used $\mu = -3.025$ to represent a gas supersaturated environment, as required experimentally to observe micropancakes. Figure 1(a) shows the grand energy Ω as a function of the vapor volume. We can observe a local minimum in the system's free energy. The corresponding state is a thermodynamically metastable state. The morphology of the metastable state shown in Fig. 1(c) surprisingly corresponds to a flat gaseous layer with the same height as the posts, reminiscent to same feature of micropancakes observed experimentally. The gaseous state will be called micro-Cassie state hereafter.

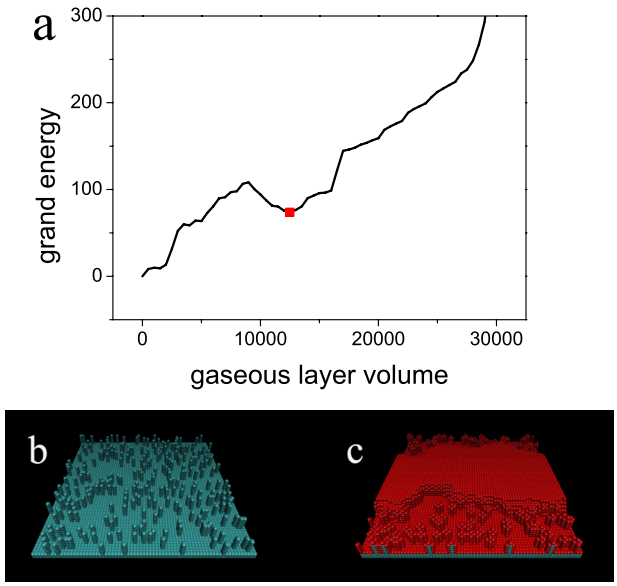

FIG. 1. (a) Grand potential difference as a function of the volume of gaseous layer. (b) The substrate with a post (area) density of 0.06 and a post height of 5. (c) The metastable Cassie-state formed on the substrate for the state indicated in Figure (a). In the figure, only the fluid particles at both liquid-solid and vapor-liquid interfaces are shown as red lattice sites for clarity.

Clearly, the nanoscale posts play an important role in stabilizing the new gaseous state. Under the same conditions, we built a series of substrates [see Fig. 2] to probe the stability mechanism of the micro-Cassie states. The substrates have 4 [Fig. 2(a)], 16 [Fig. 2(b)], 121 [Fig. 2(c)] regularly arranged posts, respectively, with a post spacing of to 4 and a post height of 7. The simulation revealed that micro-Cassie states would not be reproduced by the substrates with 4 and 16 posts. However, when the number of posts increased to 25 or more, stable flat gaseous layers were observed [Fig. 2(g)]. The morphology of the state that forms on the substrate with 121 posts is shown in Fig. 2(f).

Fig. 2(g) shows a size effect for the stability of the pancake-like micro-Cassie state. The larger gas pancakes are stabilized cooperatively by a larger number of posts, while these smaller gaseous layers can not live alone. The size dependent stability of the micro-Cassie states originates from the different fraction of gas pieces formed by neighboring posts on the boundary region, which shows less stability.

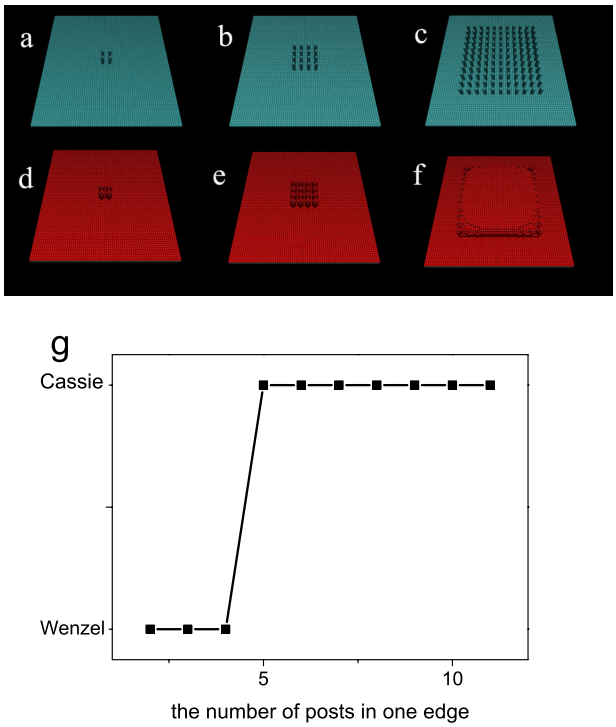

FIG. 2. The size effect of substrate roughness. The substrate has 4 (a), 16 (b), and 121 posts (c) with a height of 7 and a post spacing of 4. The corresponding states formed on substrate ((a)-(c)) are shown in ((d)-(f)), respectively. (g) indicates the transition from the Wenzel state to the Cassie state as a function of the size of substrate roughness.

To simplify the description, the gas pancake can be approximated as a quasi-two-dimensional gas layer. When a gas pancake is formed on the patterned substrate, there are two contributions to the change in the energy of the system. As a result of replacing liquid layer with gas layer, the surface energy under supersaturated environment decreases because the energy per unit area of gas layer is lower than that for the liquid layer. On the other hand, there exists a quasi-one-dimensional contact line for the gas pancake at the boundary region, and the line energy increases upon creating the new contact line. As the number of posts, N_p, increases, the change of surface energy decreases linearly with N_p, whereas the line energy increases approximately with $N_p{}^{1/2}$. Therefore, the total energy at first increases with increasing N_p before reaching a maximum value at a critical value of $N_{p,c}$, and then decreases.

From above discussion, the size dependent stability of the micro-Cassie states can be interpreted as follows. For the substrate with a small size roughness ($N_p < N_{p,c}$), the state is in the Wenzel state [Fig. 2(g)] because the small number of posts alone cannot stabilize the gaseous state. In the case of $N_p < N_{p,c}$, it is the line energy that dominates the grand potential. For the substrate with $N_p > N_{p,c}$, the surface energy dominates the grand potential, and therefore a micro-Cassie state is stabilized cooperatively by the posts. In general, our results show that the size of the rugged surface plays an important role in the transition between Wenzel and Cassie state. We find that for substrates having a number of posts that form inter-connected pores, the collective behavior of gaseous state in neighboring pores makes the existence of the Cassie state possible. Hence, we notice that the finite size effect may exist for the Wenzel to Cassie state transition for substrates having interconnected pores.[45–47]

Note that micro-Cassie states considered in this work are of a size of at most 100 nm. This is because it is hard to investigate a micron-sized system by constrained LDFT based on all molecular details. However, we explicitly considered finite size effects in this work [Fig. 2(g)] and the present results could have been extended to the micrometer scale if computational time and storage capacity had allowed.

B. Occurrence of stable micro-Cassie states

We now investigated the morphology and stability of micro-Cassie states under different conditions. It is found that the post height and spacing, the interaction strength between solid and fluid, and the chemical potential, i.e., the supersaturation here, play important roles in affecting the stability and morphology of the micro-Cassie states.

First, we studied the effect of different substrate structures on the morphology and stability of the micro-Cassie states. A post array of 10×10 with a spacing of 4 was considered, and we set $\varepsilon_{sf} = 0.3$ and $\mu = -3.025$. We increased gradually the post height from 3 to 7, and the corresponding grand energy as a function of gaseous layer volume is shown in Fig. 3(a). For the posts with a height of 3, the local minimum vanishes and the micro-Cassie state becomes unstable. However, a local minimum appears as the post height increases further and thus stable micro-Cassie states are observed.

Then, the height of the posts is fixed at 7 while increasing the post spacing from 3 to 7. The resulting change of grand energy as a function of gaseous layer volume is shown as Fig. 4(j), showing that increasing post spacing reduces the stability of the Cassie state, which reaches the limit of stability

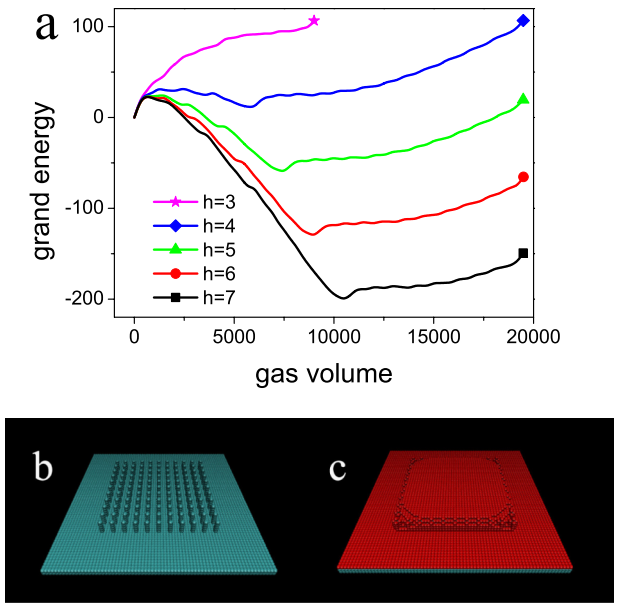

FIG. 3. (a) Grand potential difference as a function of the volume of gaseous layer. The post height ranges from 3 to 7 for a post spacing of 4. (b) A typical substrate having posts with a height of 5 and (c) the metastable micropancake formed on the substrate. In above figures, the post spacing was fixed to 4, and the zone coating with posts occupies an area of 40×40.

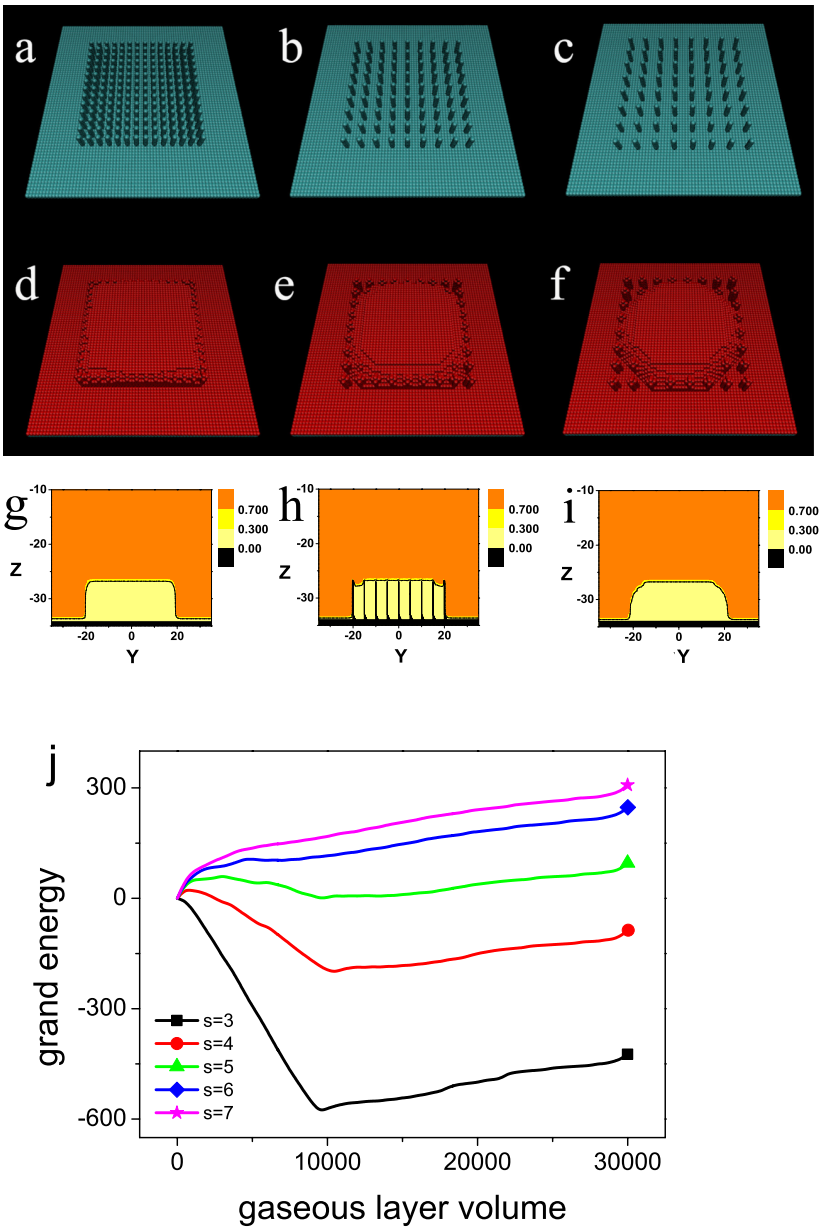

FIG. 4. ((a)-(c)) The substrates decorated with posts having a height of 7 and a spacing of 3 (a), 5 (b), and 6 (c). The region decorated with posts occupies an area of 39×39, 40×40, 42×42, for substrates ((a)-(c)), respectively. Corresponding snapshots for the metastable Cassie states formed on substrates ((a)-(c)) are shown in ((d)-(f)), along with typical cross sections for x = 0 given in density profiles ((g)-(i)). (j) gives grand potential difference as a function of gaseous layer volume.

when the post spacing is equal to 6. For the same reason, with increasing the post spacing, the boundary region of the Cassie state with less neighboring posts will collapse, and accordingly the cube-liked Cassie state will turn into a shape with rounded boundary [see Fig. 4]. This also confirms our conclusion that the formation of Cassie states is promoted by the cooperative effect of the gas piece. This observation indicates that the higher and denser roughness (posts) contributes more favorably to the stability of micro-Cassie states.

Then, we investigate the effect of the attraction between solid and fluid and of the chemical potential. In our simulations, the substrates were decorated with posts of height of 7 and spacing being range from 2 to 7, and ε_{sf} ranging from 0.2 to 0.5 and μ from −3.035 to −3.005 were considered.

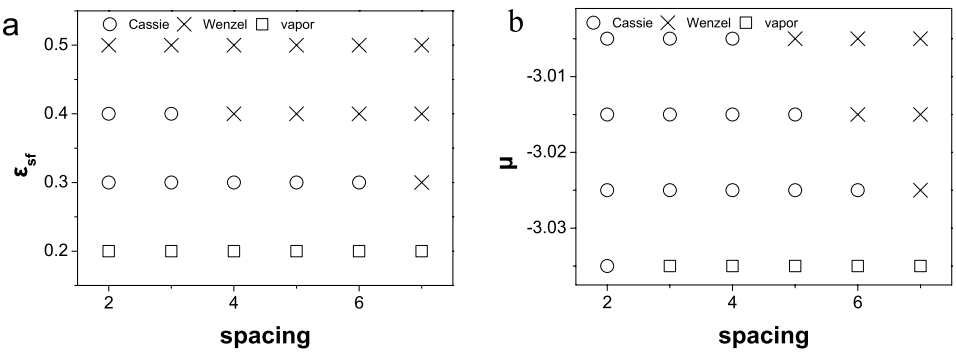

FIG. 5. The phase diagram of different interfacial states is shown (a) in the plane of post spacing and fluid-solid interaction at $\mu = -3.025$ and (b) in the plane of post spacing and chemical potential at $\varepsilon_{sf} = 0.3$.

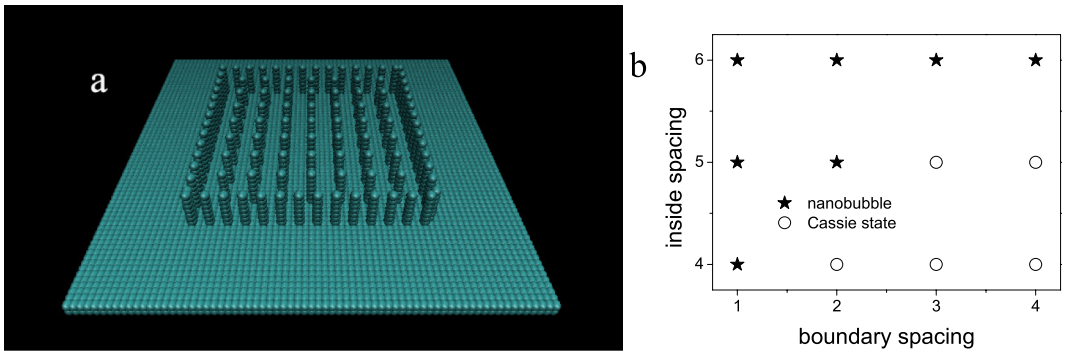

FIG. 6. (a) A typical substrate having a post spacing of 3 in the boundary region and a post spacing of 5 in the central region. (b) The phase diagram of the appearance of Cassie states and nanobubbles in the plane of boundary post spacing and central post spacing. In above figures, the height of posts was set to 7.

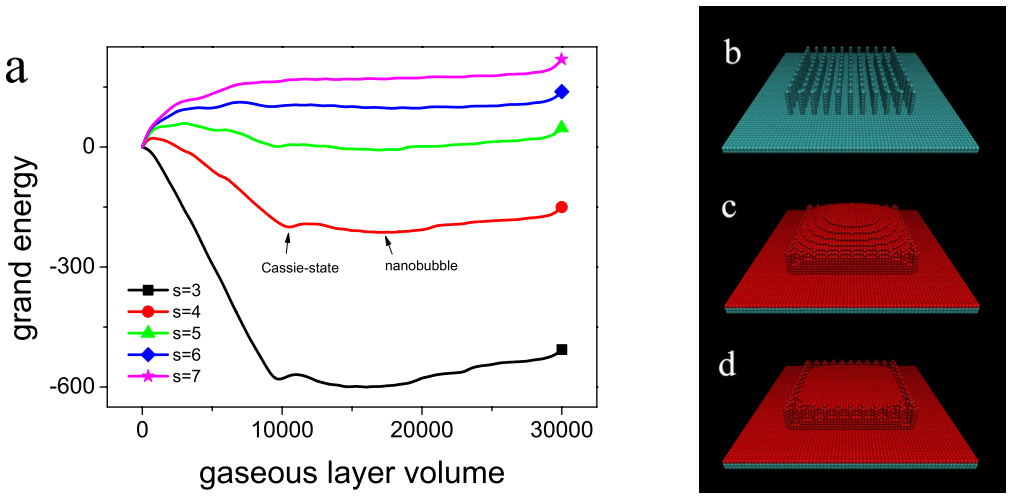

FIG. 7. (a) Grand potential difference as a function of the volume of gaseous layer formed on substrates having posts of different heights in the boundary and central regions. The post spacing ranged from 3 to 7. (b) shows a typical substrate coating with boundary posts of a height 9 and central posts of a height 7. ((c) and (d)) show the typical morphology for a nanobubble and a Cassie state indicated in figure (a). In figures ((b)-(d)), the post spacing was set to 4.

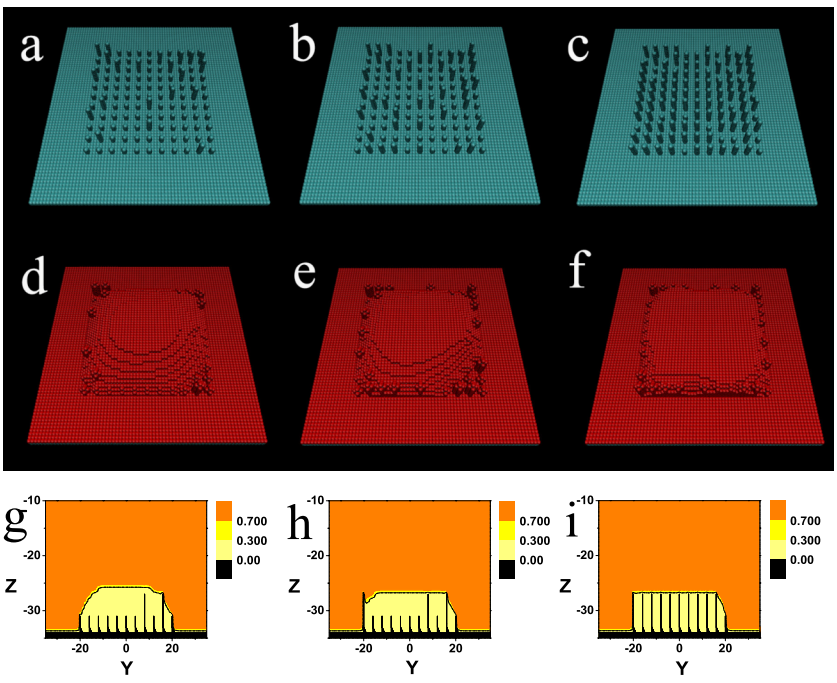

FIG. 8. ((a)-(c)) Substrates decorated with two types of posts having different heights of 7 and 3 in a region of 40×40, and area ratio for the posts was set to (a) 0.2, (b) 0.4, and (c) 0.8, respectively. Corresponding metastable Cassie states or nanobubbles formed on substrates ((a)-(c)) are given in ((d)-(f)). The density profiles are given in ((g)-(i)).

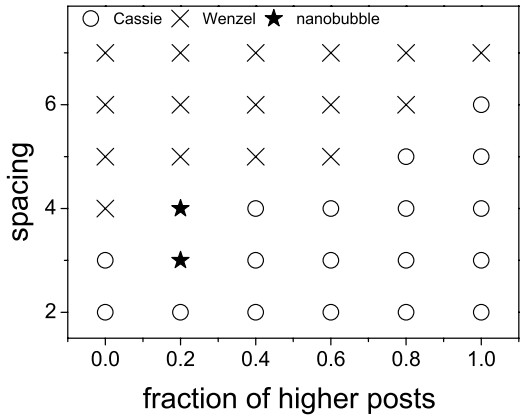

FIG. 9. The phase diagram for interfacial states in the plane of post spacing and the areal ratio for the posts having a height of 7.

Two-phase diagrams in the ε_{sf}-spacing plane and in the μ-spacing plane are constructed and shown in Fig. 5, indicating the scopes in which stable micro-Cassie states appear. When ε_{sf} or μ is sufficiently low, the liquid-to-gas phase transition occurs (see Fig. 5).

C. Different origins for micro-Cassie states and nanobubbles

Surface nanobubble stability originates from the interplay between contact line pinning[18,48] that is induced by the physics roughness or chemical heterogeneity and gas oversaturation.[14–18] The roughness was represented by pillars in the numerical work of Refs. 14–16, which, together with the gas oversaturation, led to stable surface nanobubbles. In the related numerical models of this present work, the physical roughness is modeled in a similar way and it is the prerequisite for stable micro-Cassie states, again together with the gas oversaturation. Thus, the question arises: what is the difference between the two types of roughness that induce respectively nanobubbles and micro-Cassie states? Our above simulations show that when the spacing of posts ranges from 4 to 6, the micro-Cassie state can live [see Fig. 4(j)]. Further, we intensified the boundary effect by decreasing the spacing of posts (S = 1–4) located in the boundary region as shown in Fig. 6(a) under the conditions of $\varepsilon_{sf} = 0.3$ and $\mu = -3.025$. The phase diagram [see Fig. 6(b)] indicates that the micro-Cassie states would turn to nanobubbles if we decrease the spacing of posts in the boundary region. It seems more beneficial to the nanobubble formation when the substrate owns denser posts in the boundary and sparser ones in the central region.

In general, our simulations demonstrate that if the nanoscale roughness in the boundary region is sufficiently dense and the surface roughness inside the central area is sparse, the boundary effect produces a strong pinning effect and nanobubbles form more easily. On the other hand, if the roughness inside strengthens while the boundary effect becomes weakened, the Cassie state will form instead. Therefore, it is the competition between roughness near the boundary region and that inside the central region that determines the appearance of the different gaseous states.

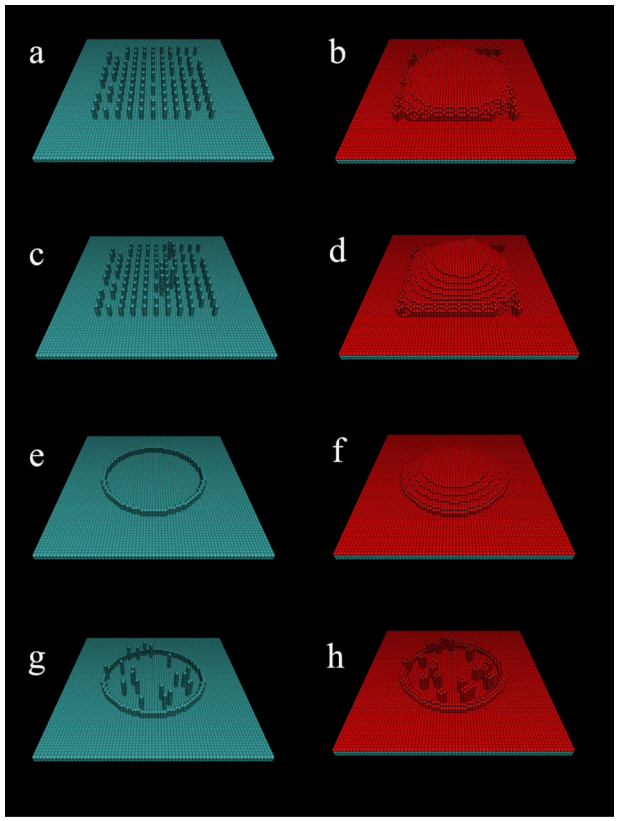

FIG. 10. ((a) and (b)) The substrate (a) and the corresponding gaseous structure formed (b). The substrate was constructed initially with regularly arranged posts with a height of 5 and a spacing of 4, followed by 20% of the posts being randomly chosen and removed. ((c) and (d)) The substrate (c) and the corresponding gaseous state formed (d). The substrate (c) was modified from substrate (a) for which several higher posts with a height of 10 were added. ((e) and (f)) The substrate decorated with a ring of boundary posts (e) and the corresponding gaseous state formed (f). ((g) and (h)) The substrate (g) and the corresponding interfacial state (h). The substrate (g) was obtained via adding several higher posts with a height 7 inside the central region of the substrate (e), and (h) indicates the disappearance of the nanobubble. In figures ((a)-(d)), we chose $\varepsilon_{sf} = 0.3$ and $\mu = -3.025$, and the area occupied by posts is 40×40. Whereas in figures ((e)-(h)), we chose $\varepsilon_{sf} = 0.5$ and $\mu = -3.025$, and the ring-like boundary is of a height of 3 and a radius of 20.

In order to further support our conclusion, we also build a series of substrates with the same post spacing from 3 to 7, but the post height are 9 and 7, respectively, in boundary and central region, as shown in Fig. 7(b). In this case, the calculated grand energy as a function of the gas volume shows two local minima that represent, respectively, the metastable nanobubble and the Cassie state [see Fig. 7(a)]. The local minimum for nanobubble is deeper than that for the Cassie state, indicating that the nanobubble is more stable because taller boundary posts provide a strong pinning effect that contributes to the formation of nanobubbles.

D. The effect of substrates with different types of roughness

In order to mimic the solid surfaces with roughness of different heights, we constructed substrates having two types of posts with a height of 3 and 7, respectively. Different posts were chosen randomly and placed regularly on a region of the substrate that has a area of 40×40 (see Fig. 8), with a

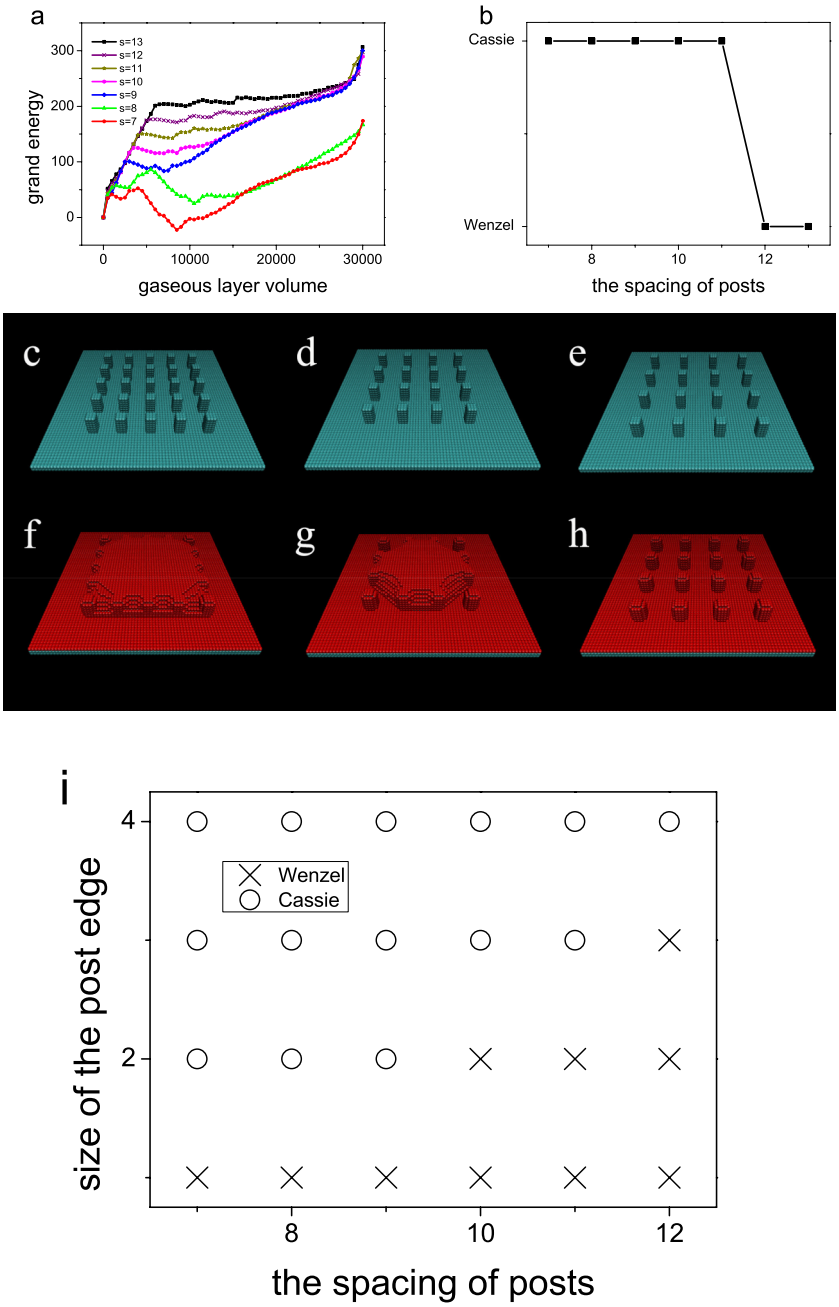

FIG. 11. The size of the posts has an effect of the Cassie-state stability. (a) Grand potential difference as a function of the volume of gaseous layer. The height of the posts is 7 and the post size is 3×3. The number of posts with the case of spacing being 7 and 8 is 25 and the others is 16. The obtained snapshots show that micro-Cassie states are stable for the substrates with a post spacing of 8 ((c) and (f)), 10 ((d) and (g)) and become unstable at 12 ((e) and (h)). (b) The transition from the Cassie to the Wenzel state as the post spacing increases. (i) The phase diagram for the interfacial states in the plane of post spacing and the size of the posts.

post spacing of 4. Again, we set $\varepsilon_{sf} = 0.3$ and $\mu = -3.025$. We changed the ratio of these two types to find out its effect on the morphology and stability of micro-Cassie states under different conditions. From the Fig. 8, we can find that as the fraction of height 7 posts decreases from 0.8 to 0.2, the Cassie state becomes increasingly unstable. The boundary of the micro-Cassie state will collapse and become irregular. Moreover, when the fraction decreases to 0.2, the centre of the micro-Cassie state will grow and exceed the height of taller posts and in this case, the Cassie state transforms to a nanobubble. In this case, it is the boundary effect that becomes the dominating factor and thus induces nanobubbles.

Our above simulations indicate the essential role of taller posting in stabilizing micro-Cassie states. To identify the effect of shorter ones, we removed the shorter posts from the substrates in the case of the fraction of taller post equal to 0.5, and neither the micro-Cassie state nor nanobubble was found. This observation shows that although the taller posts play the key factor, the shorter ones also have a significant effect on stabilizing micro-Cassie states. There exists a complicated cooperative effect between taller and shorter posts, both of which together stabilize the Cassie state.

The stability phase diagram is shown in Fig. 9. The same conclusion can be obtained from that figure, that is, increasing spacing leads to a weakened stability of the micro-Cassie states. In our simulations, we also find the existence of nanobubbles. For example, we find that sparely distributed higher posts would weaken the stability of micro-Cassie states and results in the formation of nanobubbles, as shown in Fig. 8(g).

Therefore, we constructed several special substrates [see Fig. 10] to confirm this point. We put a few of the higher

posts into the initial substrates shown in Figs. 10(a) and 10(e) randomly, and the new substrates are shown in Figs. 10(c) and 10(g), respectively. The results indicate that a few higher posts that mismatch the shape of micro-Cassie states and nanobubbles weaken the stability of the gaseous states and lead to the state change or disappearance. For the micro-Cassie state [Fig. 10(b)], the addition of taller posts turns the Cassie state into nanobubble [Fig. 10(d)]. While for nanobubbles [Fig. 10(f)], introduction of a few higher posts protruding above the nanobubble would induce the disappearance of nanobubbles [Fig. 10(h)]. In general, the presence of roughness that mismatches with micro-Cassie states tends to weaken the stability of the gaseous state and inhibit its formation.

We finally show that the micro-Cassie states can be stabilized by sparser but larger substrate roughness (Fig. 11). When we increased the post size from 1×1 to 3×3, a larger post spacing required for stable micro-Cassie states is found, namely, a sparser roughness is needed, as indicated by Figs. 11(a)–11(h). Then, we systematically changed the post size and post spacing, and the corresponding phase diagram for the stability of different wetting states is obtained [see Fig. 11(i)]. Again, the figure shows that the roughness of the substrate plays the key of the stability of the micro-Cassie states. Furthermore, it also indicates that the maximum post spacing required for stable micro-Cassie states increases with the post size. In other words, the micro-Cassie states can be stabilized by sparser and less peaky roughness.

E. Similarity between micro-Cassie states and micropancakes

Our simulation results on the micro-Cassie states show some similar features to the micropancakes observed experimentally, i.e., flat and pancake-shaped gaseous layers with a larger size than nanobubbles as well as supersaturated environment required.[16] With the stability mechanism proposed above, some behaviors of micropancakes obtained from experimental observations, such as lateral diffusion of micropancakes and the formation of nanobubble-micropancake composite, can be reproduced from the micro-Cassie states investigated in this work. The lateral diffusion is one of the particular characteristics of micropancakes.[19] Experiments demonstrate that small micropancakes can spread and combine together to form larger ones. Here, we built a substrate having two post arrays, which are connected with a neck having sparse posts [see Fig. 12(a)]. The height of posts was 7, and ε_{sf} and μ were set to 0.3 and −3.025, respectively. The grand energy as a function of gas volume shows two local minimum [see Fig. 12(b)]. From the morphology of the metastable states [Figs. 12(c) and 12(d)], we can find that along with the gas volume increases, the micro-Cassie state can live in one array and then spread to the other. In particular, both of them are stable.

Another particular characteristic of micropancakes is the composite structure comprising nanobubble sitting on a micropancake.[19] In our opinion, the formation of nanobubbles and micro-Cassie states needs to obey different requirements for substrate roughness in the boundary region and in the central region. Hence, we design a substrate structure with 3 types of roughness. A perforated circle-shape roughness with

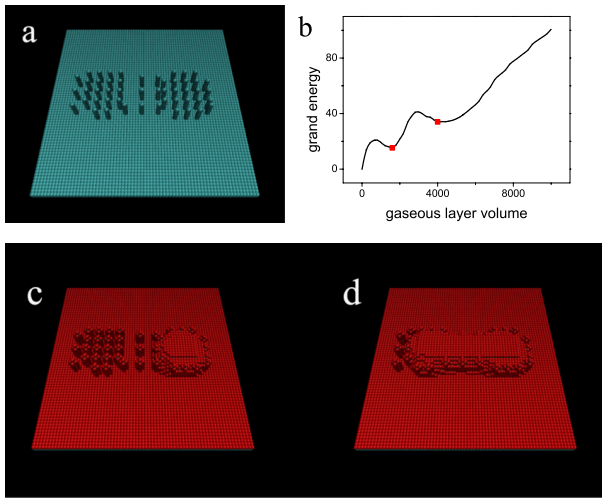

FIG. 12. (a) The substrate decorated with two regions of high post density that are connected by a neck with lower post density. (b) Grand potential difference as a function of the volume of gaseous layer formed on the substrate. Local grand potential minima are also indicated in the figure, which correspond to formation of (c) a small micropancake and (d) a larger one, respectively.

a radius of 20 is introduced to act as the boundary region that induces the pinning effect to stabilize a nanobubble. Then, some posts were randomly introduced mainly in a particular region to stabilize micro-Cassie states [Fig. 13(b)]. The post density in the denser region (outside the boundary), in the particular boundary region, and in sparser region (inside the boundary) is 0.1, 0.8, and 0.02, respectively [see Fig. 13(b)]. Fig. 13(a) shows the grand potential as a function of gas volume. The morphology for the state with the local free energy minimum corresponds to the composite of nanobubble and micro-Cassie state [see Fig. 13(c)], analogous to the nanobubble-micropancake composite observed experimentally.

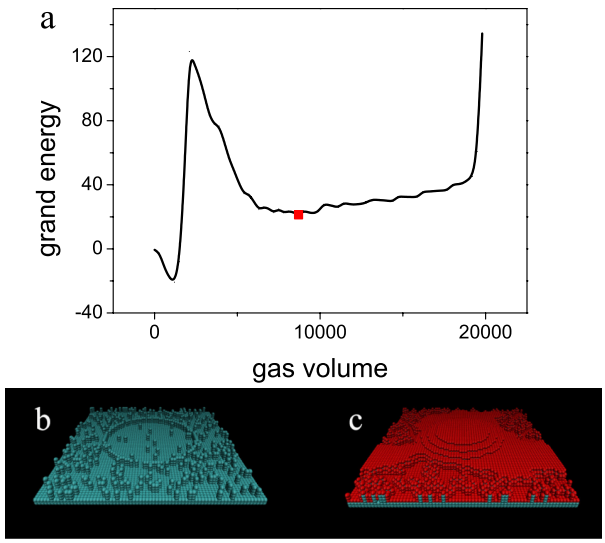

FIG. 13. (a) Grand potential difference as a function of the volume of the gaseous layer formed on a substrate shown in (b). (c) shows the metastable nanobubble-micropancake composite formed at the state marked in figure (a). The substrate decorated with the ring-like structure, which has a post density of 0.8, and with posts having a density of 0.02 inside the ring and a density of 0.1 outside.

From the above similarity between the micro-Cassie state obtained in this work and micropancakes from experimental observations, one may be tempted to regard micropancakes as large-sized micro-Cassie states, the stability of which depends on the size of the surface roughness. The general trend of micro-Cassie states from our simulations is similar to that of micropancakes from various experimental studies. First of all, recent studies on surface nanobubbles/nanodroplets have highlighted the importance of surface heterogeneity on a molecular level.[15,17,18,49,50] Similarly, we suggest here that typical micro-Cassie states are also ascribed to surface heterogeneities (physical roughness). Such heterogeneities for micropancakes may originate from substrate processing or airborne adsorbents.

In previous experimental work, a similar form of interfacial gaseous domains, thin gas layers, was observed on rough hydrophobic salinized silicon that was decorated with high number density of tiny particles.[27] The thin gas layers were thought to be different from the typical micropancakes on HOPG and other crystalline substrates. But based on the stability mechanism proposed here, those gaseous states share some similarities, in particular all of them are stabilized by substrate roughness. Our simulations reveal that denser posts on the surface are favorable for the stability of micro-Cassie states, similar to the formation of thin gas layers on the hydrophobic salinized Si with many small particles or densely distributed scratches, but not on smooth salinized Si.[27]

The observation from the simulations is that the presence of roughness that mismatches with the height of micro-Cassie states tends to weaken the stability of the gaseous state and inhibits its formation. This might be put into the context of experimental observations that micropancakes can only be produced on HOPG and glassy carbon,[27] but not on amorphous carbon.[27] HOPG is of controllable roughness on atomically flat substrate between the cleavage steps, while the amorphorous carbon has uncontrollable roughness.

IV. CONCLUSIONS

In summary, our model calculations with the CLDFT show that small and individual micro-Cassie state surrounded by the model surface roughness of a few posts cannot live alone. However, the collective interaction with their neighbors induces the formation of larger stable Cassie states, which is enhanced by the taller and denser posts and the regular distribution of post height but is inhibited by the roughness that mismatches with the height of the gaseous domains. Our simulations also demonstrate that if the nanoscale roughness in the boundary region is sufficiently denser and the surface roughness inside the central area is relatively sparser, the boundary effect produces a strong pinning effect and surface nanobubbles form more easily. On the other hand, if the roughness inside strengthens while the boundary effect becomes weakened, micro-Cassie states form instead.

ACKNOWLEDGMENTS

This work is supported National Natural Science Foundation of China (Grant Nos. 21276007 and 91434204). X.H.Z. acknowledges the support from the Australian Research Council (Grant Nos. FT120100473 and DP140100805) and D.L. and X.H.Z. acknowledge support from the MCEC programme, sponsored by NWO.

[1]S.-T. Lou, Z.-Q. Ouyang, Y. Zhang, X.-J. Li, J. Hu, M.-Q. Li, and F.-J. Yang, J. Vac. Sci. Technol., B **18**, 2573 (2000).
[2]R. Steitz, T. Gutberlet, T. Hauss, B. Klosgen, R. Krastev, S. Schemmel, A. C. Simonsen, and G. H. Findenegg, Langmuir **19**, 2409 (2003).
[3]K. Ohgaki, N. Q. Khanh, Y. Joden, A. Tsuji, and T. Nakagawa, Chem. Eng. Sci. **65**, 1296 (2010).
[4]R. Becker and W. Döring, Ann. Phys. **416**, 719 (1935).
[5]D. W. Oxtoby and R. Evans, J. Chem. Phys. **89**, 7521 (1988).
[6]X. Zeng and D. W. Oxtoby, J. Chem. Phys. **94**, 4472 (1991).
[7]M. P. Brenner and D. Lohse, Phys. Rev. Lett. **101**, 214505 (2008).
[8]J. R. T. Seddon, H. J. W. Zandvliet, and D. Lohse, Phys. Rev. Lett. **107**, 116101 (2011).
[9]E. Dietrich, H. J. W. Zandvliet, D. Lohse, and J. R. T. Seddon, J. Phys.: Condens. Matter **25**, 184009 (2013).
[10]F. Caupin and E. Herbert, C. R. Phys. **7**, 1000 (2006).
[11]X. H. Zhang, M. H. Uddin, H. J. Yang, G. Toikka, W. Ducker, and N. Maeda, Langmuir **28**, 10471 (2012).
[12]W. A. Ducker, Langmuir **25**, 8907 (2009).
[13]H. Peng, G. R. Birkett, and A. V. Nguyen, Langmuir **29**, 15266 (2013).
[14]Y. W. Liu, J. J. Wang, X. R. Zhang, and W. C. Wang, J. Chem. Phys. **140**, 054705 (2014).
[15]Y. W. Liu and X. R. Zhang, J. Chem. Phys. **138**, 014706 (2013).
[16]Y. W. Liu and X. Zhang, J. Chem. Phys. **141**, 134702 (2014).
[17]D. Lohse and X. H. Zhang, Phys. Rev. E **91**, 031003(R) (2015).
[18]J. H. Weijs and D. Lohse, Phys. Rev. Lett. **110**, 054501 (2013).
[19]X. H. Zhang, X. D. Zhang, J. L. Sun, Z. X. Zhang, G. Li, H. P. Fang, X. D. Xiao, X. C. Zeng, and J. Hu, Langmuir **23**, 1778 (2007).
[20]X. H. Zhang, N. Maeda, and J. Hu, J. Phys. Chem. B **112**, 13671 (2008).
[21]X. Zhang and D. Lohse, Biomicrofluidics **8**, 041301 (2014).
[22]Y. H. Lu, C. W. Yang, and I. S. Hwang, Appl. Surf. Sci. **304**, 56 (2014).
[23]H. An, G. Liu, and V. S. Craig, "Wetting of nanophases: Nanobubbles, nanodroplets and micropancakes on hydrophobic surfaces," Adv. Colloid Interface Sci. (in press).
[24]H. Peng, M. A. Hampton, and A. V. Nguyen, Langmuir **29**, 6123 (2013).
[25]Y. H. Lu, C. W. Yang, and I. S. Hwang, Langmuir **28**, 12691 (2012).
[26]J. R. T. Seddon and D. Lohse, J. Phys.: Condens. Matter **23**, 133001 (2011).
[27]X. Zhang and N. Maeda, J. Phys. Chem. C **115**, 736 (2010).
[28]J. R. Seddon, O. Bliznyuk, E. S. Kooij, B. Poelsema, H. J. Zandvliet, and D. Lohse, Langmuir **26**, 9640 (2010).
[29]L. J. Zhang, X. H. Zhang, C. H. Fan, Y. Zhang, and J. Hu, Langmuir **25**, 8860 (2009).
[30]C. L. Wang, Z. X. Li, J. Y. Li, P. Xiu, J. Hu, and H. P. Fang, Chin. Phys. B **17**, 2646 (2008).
[31]Z. Li, X. Zhang, L. Zhang, X. Zeng, J. Hu, and H. Fang, J. Phys. Chem. B **111**, 9325 (2007).
[32]Y. M. Men, X. R. Zhang, and W. C. Wang, J. Chem. Phys. **131**, 184702 (2009).
[33]V. Talanquer and D. W. Oxtoby, J. Chem. Phys. **100**, 5190 (1994).
[34]A. Haymet and D. W. Oxtoby, J. Chem. Phys. **74**, 2559 (1981).
[35]Y. M. Men, Q. Z. Yan, G. F. Jiang, X. R. Zhang, and W. C. Wang, Phys. Rev. E **79**, 051602 (2009).
[36]Y. M. Men and X. R. Zhang, J. Chem. Phys. **136**, 124704 (2012).
[37]S. Auer and D. Frenkel, Nature **409**, 1020 (2001).
[38]Y. M. Men, X. R. Zhang, and W. C. Wang, J. Chem. Phys. **134**, 124704 (2011).
[39]D. Zhou, M. Zeng, J. G. Mi, and C. L. Zhong, J. Phys. Chem. B **115**, 57 (2011).
[40]Z. D. Li and J. H. Wu, Ind. Eng. Chem. Res. **47**, 4988 (2008).
[41]Q. M. Guo, Y. W. Liu, G. F. Jiang, and X. R. Zhang, J. Chem. Phys. **138**, 214701 (2013).
[42]Y. W. Liu, Y. M. Men, and X. R. Zhang, J. Chem. Phys. **135**, 184701 (2011).
[43]Y. W. Liu, Y. M. Men, and X. R. Zhang, J. Chem. Phys. **137**, 104701 (2012).
[44]Y. W. Liu and X. R. Zhang, Phys. Rev. E **88**, 012404 (2013).
[45]E. Bormashenko, R. Pogreb, G. Whyman, and M. Erlich, Langmuir **23**, 6501 (2007).
[46]T. Koishi, K. Yasuoka, S. Fujikawa, T. Ebisuzaki, and X. C. Zeng, Proc. Natl. Acad. Sci. U. S. A. **106**, 8435 (2009).
[47]P. Tsai, R. G. H. Lammertink, M. Wessling, and D. Lohse, Phys. Rev. Lett. **104**, 116102 (2010).
[48]X. H. Zhang, D. Y. C. Chan, D. Y. Wang, and N. Maeda, Langmuir **29**, 1017 (2013).
[49]A. Checco, P. Guenoun, and J. Daillant, Phys. Rev. Lett. **91**, 186101 (2003).
[50]C. Xu, S. Peng, G. G. Qiao, V. Gutowski, D. Lohse, and X. Zhang, Soft Matter **10**, 7857 (2014).